Intralesional Characteristics of Correlated 18-Fluorodeoxyglucose PET and Intravoxel Incoherent Motion Parameters in Locally Advanced Breast Cancer

Jason Ostenson[1], Linda Moy[1], Sungheon G. Kim[1], Amy Melsaether[1], Komal Jhaveri[2], Christian Geppert[3], David Faul[3], Francisco Esteva[2], Sylvia Adams[2], Freya Schnabel[4], Kimberly Jackson[1], Joon Lee[1], Christopher Glielmi[3], Gene Young Cho[1,5], Thorsten Feiweier[6], and Eric E. Sigmund[1]

[1]Department of Radiology, NYU Langone Medical Center, New York, NY, United States, [2]Perlmutter Cancer Center, NYU Langone Medical Center, New York, NY, United States, [3]Siemens Medical Solutions, New York, NY, United States, [4]Department of Surgery, NYU Langone Medical Center, New York, NY, United States, [5]Sackler Institute of Graduate Biomedical Sciences, NYU School of Medicine, New York, NY, United States, [6]Siemens AG, Erlangen, Germany

Target Audience: Scientists and clinicians interested in the application of diffusion-weighted imaging (DWI) and PET in breast cancer.

Purpose: Diffusion-weighted MRI [1-4] and 18-fluorodeoxyglucose(FDG)-PET [5-8] are powerful but distinct probes of breast cancer aggressiveness. The behavior of the tumor microenvironment needs further exploration to understand how restricted diffusion, perfusion, and glucose metabolism interrelate. This study exploits simultaneously acquired DWI and FDG-PET of locally advanced breast cancer to evaluate the correlations between SUV and markers of both diffusion and perfusion on a voxelwise basis. The resulting correlated metrics are used to derive classifications that may provide new categorizations of tumor heterogeneity.

Methods: In this IRB-approved, HIPAA-compliant study 15 women aged 24 to 65 years with histopathologically proven breast cancer were imaged with a whole-body integrated 3T MR/PET system (Biograph mMR, Siemens AG, Erlangen, Germany) following a clinical FDG-PET/CT. One woman was imaged before and after chemotherapy making a total of 16 imaged index lesions. DWI employed a prototype twice-refocused spin echo EPI sequence with inline eddy-current distortion correction and SPAIR with extra fat suppression at 10 b-values ($0 < b < 800$ s/mm^2) with a dedicated 4-channel breast coil [9]. The FDG-PET acquisition used a single thorax position beginning an average of 170 min following the FDG injection for the clinical PET/CT exam. Each subject was then injected with gadoteridol (ProHance) and imaged using a standard Cartesian k-space T1w-GRE (VIBE) or prototype golden angle radial sparse parallel (GRASP) protocol to yield a T1 post-contrast image. The PET images were reconstructed using 3D OP-OSEM, MR VIBE in/out phase imaging and a prototype breast coil μmap [9] for attenuation correction. The index lesion on each T1 image volume was contoured using MIM (MIM Software, Cleveland, OH) and then used as a reference to manually co-register the PET and DWI volumes to one another with rigid body translation (Fig 1) by a single observer blinded to pathology. This registration correction served to compensate for spatial distortion in the DWI. The co-registered PET and DWI sequences were exported to IGOR Pro (WaveMetrics, Lake Oswego, OR) to derive apparent diffusion coefficient (ADC) and intravoxel incoherent motion (IVIM) [10] parameter maps of tissue diffusion (D_t), perfusion fraction (f_p), and pseudo-diffusion (D_p), which are key indicators of aggressiveness in breast cancer [11-14]. The parametric maps of each contoured lesion were used to create a joint (2D) histogram for SUV vs. D_t and f_p. These histograms were analyzed visually and Pearson's correlations were calculated for the two SUV-DWI metric pairs to categorize the lesions. Finally, each lesion's voxels were divided into three groups of malignancy according to each voxel's value relative to lesion mean SUV, D_t, and f_p: (1/most malignant) above average (avg.) SUV, lower than avg. D_t, above avg. f_p; (2/least malignant) below avg. SUV, above avg. D_t, below avg. f_p; and (3/intermediate malignancy) not falling into (1) or (2). Voxels that could not be fit in either D_t or f_p were not assigned a group. Joint histogram typing and fractional volume contributions in each of the three lesion subgroups were calculated and compared with therapeutic history, metastatic burden, and prognostic factors of estrogen/progesterone receptor (ER/PR), proliferation factor (Ki-67), and Her2/neu expression.

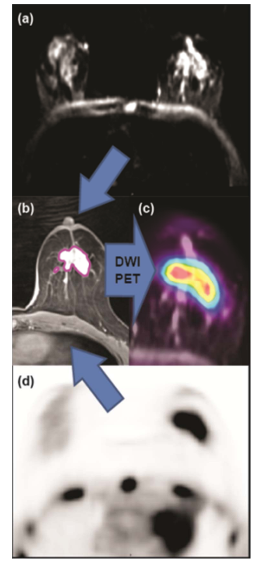

Fig 1. An axial slice from the DWI (a) and PET (d) are co-registered via the T1 post contrast (b) so that they are spatially correlated on a voxel-by-voxel basis (c).

Results: The lesions consisted of seven IDC, four IDC/DCIS, three ILC, and one adenocarcinoma not otherwise specified. The 2D histograms of SUV with D_t and SUV with f_p (Fig 2) in conjunction with Pearson's correlation revealed three classifications. One set of six lesions' histograms exhibited a negative correlation in SUV vs. D_t and a weakly positive or negative correlation in SUV vs. f_p (r = 0.2 to -0.15) categorized Type A. Seven lesions, categorized Type B, showed a negative correlation in SUV vs. D_t but often exhibited a stronger limiting D_t and a stronger negative correlation in SUV vs. f_p than Type As. Three lesions, labeled Type C, were either small or too heterogeneous to classify with joint histograms/correlations and had positive SUV vs. D_t correlations ($r > 0.15$). The lesion imaged before and after chemotherapy changed from Type A to B. The intralesional segmentation showed that group (3)'s fraction averaged 0.56 (with standard deviation 0.09) compared to 0.09 (0.05) and 0.13 (0.05) for groups (1) and (2), respectively. Neither the most (1) nor least (2) malignant groups correlated with clinical endpoints/prognostic factors, but the remaining intermediate malignancy group (3)'s fraction significantly correlated ($p < 0.05$) with ER and Ki-67 (Spearman's rank correlation ρ = -0.6 and 0.6, respectively).

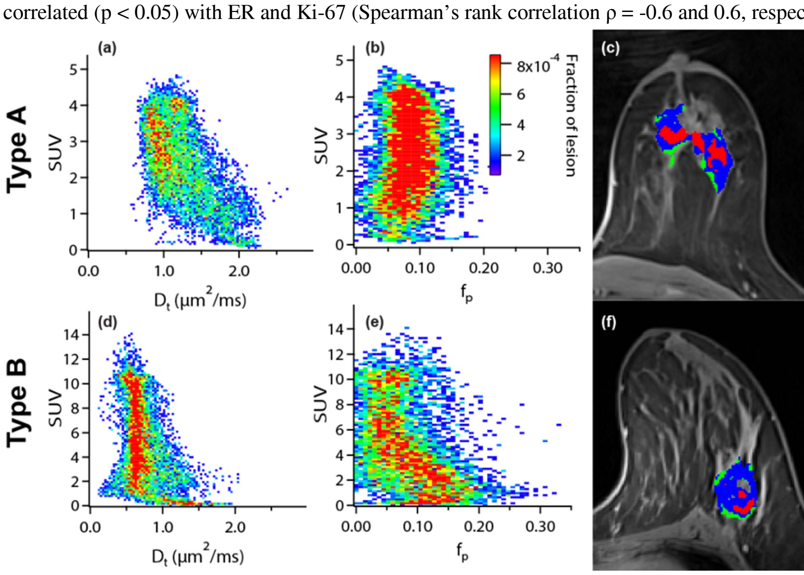

Fig 2. The joint histograms of SUV vs. D_t and SUV vs. f_p of Type A (a),(b) and B (d),(e) lesions. The intralesional segmentation of the same Type A (c) and Type B (f) are shown with canonically most malignant in red, least malignant in green, and intermediate malignancy in blue overlaid on the T1. Voxels within the lesion that could not be fit in at least one diffusion/perfusion parameter are uncolored.

Discussion: The 2D histograms allow for easy visualization of a lower threshold for diffusion as a function of FDG avidity, showing that not all lesions are identical in their metabolic function as they approach a maximum achievable cellular packing. The distribution of lesions into Types A and B by joint histogram/correlation analysis reinforces that diffusion, perfusion, and glucose uptake throughout lesions of breast cancer is heterogeneous in nature. The perfusion fraction, which correlates with microvascular density, at high relative SUV values typically showed lower relative values in some lesions (Type B) than in others (Type A). The intralesional segmentation shows that the canonically most malignant region (a) is not the majority component and (b) does not seem to reveal correlates with established clinical prognostics, but those regions that are intermediate in their SUV, D_t, and f_p relative to the lesion do correlate with such markers. This suggests that DWI and PET parameters may be able to detect metabolic and microstructural components of breast cancer that reveal the underlying phenotypical nature of breast cancer. Lastly, the change of the lesion type in the case with chemotherapy alludes to underlying changes in the tumor heterogeneity that may be tapped as imaging biomarkers to assess treatment response.

References: 1. Jeh et al. Journal of Magnetic Resonance Imaging 2011. 2. Fornasa et al. Radiologia Medica 2011. 3. Razek et al. Nmr in Biomedicine 2010. 4. Yoshikawa et al. Radiation Medicine 2008. 5. Buck et al. European Journal of Nuclear Medicine and Molecular Imaging 2004. 6. Kurland et al. EJNMMI Research 2012. 7. Groheux et al. J Nucl Med 2012. 8. Cheng et al. Acta Radiologica 2012. 9. Aklan et al. Med Phys 2013. 10. Lebihan et al. Radiology 1988. 11. Sigmund et al. Magnetic Resonance in Medicine 2011. 12. Bokacheva et al. J Magn Reson Imaging 2014. 13. Liu et al. European Journal of Radiology 2013. 14. Iima et al. Investigative radiology 2014.